Leak current, even with gigaohm seals, can cause misinterpretation of stem cell-derived cardiomyocyte action potential recordings

Alexander P. Clark[1], Michael Clerx[2], Siyu Wei[3], Chon Lok Lei[4,5], Teun P. de Boer[6], Gary R. Mirams[2], David J. Christini[1,3], Trine Krogh-Madsen[7,8]

[1] Department of Biomedical Engineering, Cornell University, Ithaca, New York, USA.

[2] Centre for Mathematical Medicine & Biology, School of Mathematical Sciences, University of Nottingham, Nottingham, UK.

[3] Department of Physiology and Pharmacology, SUNY Downstate Health Sciences University, Brooklyn, New York, USA.

[4] Institute of Translational Medicine, Faculty of Health Sciences, University of Macau, Macau, China.

[5] Department of Biomedical Sciences, Faculty of Health Sciences, University of Macau, Macau, China.

[6] Department of Medical Physiology, Division of Heart and Lungs, University Medical Center Utrecht, Utrecht, The Netherlands.

[7] Department of Physiology & Biophysics, Weill Cornell Medicine, New York, New York, USA.

[8] Institute for Computational Biomedicine, Weill Cornell Medicine, New York, New York, USA.

Corresponding Author:

Trine Krogh-Madsen

Department of Physiology & Biophysics

1300 York Avenue

Box 75; Room LC501G

New York, NY 10065

trk2002@med.cornell.edu

Abstract

Background and Aims: Human induced pluripotent stem cell-derived cardiomyocytes (iPSC-CMs) have become an essential tool to study arrhythmia mechanisms. Much of the foundational work on these cells, and the computational models built from the resultant data, has overlooked the contribution of seal-leak current on the immature and heterogeneous phenotype that has

come to define these cells. The aim of this study is to understand the effect of seal-leak current on recordings of action potential (AP) morphology.

Methods: APs were recorded in human iPSC-CMs using patch clamp and simulated using previously published mathematical models.

Results: Our *in silico* and *in vitro* studies demonstrate how seal-leak current depolarises APs, substantially affecting their morphology, even with seal resistances (R_{seal}) above 1 GΩ. We show that compensation of this leak current is difficult due to challenges with obtaining accurate measures of R_{seal} during an experiment. Using simulation, we show that R_{seal} measures: 1) change during an experiment, invalidating the use of pre-rupture values, and 2) are polluted by the presence of transmembrane currents at every voltage. Finally, we posit that the background sodium current in baseline iPSC-CM models imitates the effects of seal-leak current and is increased to a level that masks the effects of seal-leak current on iPSC-CMs.

Conclusion: Based on these findings, we make recommendations to improve iPSC-CM AP data acquisition, interpretation, and model-building. Taking these recommendations into account will improve our understanding of iPSC-CM physiology and the descriptive ability of models built from such data.

Keywords

Induced pluripotent stem cells, Patch clamp, Arrhythmias, Ion channels, Computer simulation

What's new?

- Human induced pluripotent stem cell-derived cardiomyocytes (iPSC-CMs) are an emerging tool in the study of cardiac arrhythmia mechanisms.

- Their immature and heterogeneous action potential phenotype complicates the interpretation of experimental data and has slowed their acceptance in industry and academia.
- We suggest that the leak current caused by imperfect pipette-membrane seal during single-cell patch-clamp experiments is partly responsible for causing this heterogeneity and the appearance of immaturity.
- Using *in vitro* experiments and computational modelling, we show that this seal-leak current affects iPSC-CM AP morphology, even under 'ideal' experimental conditions.
- Based on these findings, we make recommendations that should be considered when interpreting, analysing and fitting iPSC-CM data.

1 Introduction

Human induced pluripotent stem cell-derived cardiomyocytes (iPSC-CMs) are a renewable and cost-effective model for studying genetic disease mechanisms,[1,2] drug cardiotoxicity,[3] and inter-patient variability.[4] Computational approaches have been developed to translate experimental results from iPSC-CMs to make predictions in adult cardiomyocytes.[5] Such work attempts to bridge the critical gap that remains between the physiology of iPSC-CMs and excised adult human cardiac cells.

While iPSC-CMs have transformed many areas of cardiac arrhythmia research, phenotypic heterogeneity and immaturity continue to stymie their potential impact.[6,7] Investigating sources of these limitations and their biological implications is important as iPSC-CMs (and mechanistic models describing their behaviour) are used to inform increasingly complex clinical decisions.[8,9] Studies of iPSC-CMs in a single-cell patch-clamp context have indicated that their depolarised,

highly varying resting membrane potential is primarily due to decreased inward rectifier potassium current (I_{K1}) and increased funny current (I_f) compared to adult cardiomyocytes.[10]

Recently, findings from Horváth et al.[11] and Van de Sande et al.[12] indicate that the heterogeneous and depolarised resting membrane potential is also due, far more than previously thought, to a simple seal-leak current (I_{leak}). Relative to electrically coupled iPSC-CMs, they show a substantial depolarisation in the resting membrane potential in isolated iPSC-CMs despite some cells having similar I_{K1} densities to human adult cardiomyocytes.[11] These findings indicate that I_{leak} plays an important role in iPSC-CM AP morphology during single-cell patch-clamp experiments.

I_{leak} is inversely proportional to the seal resistance (R_{seal}) formed between the micropipette tip and cell membrane during patch-clamp experiments. A sufficiently large R_{seal} is expected to limit I_{leak}'s effect on AP morphology. Upon reviewing single-cell electrophysiological iPSC-CM studies, including those used to build iPSC-CM computational models,[13–15] we found that studies either do not report Rseal,[10,16–19] report a > 1 GΩ R_{seal} acceptance criteria,[20] or an average R_{seal} < 3 GΩ.[11,12]

In this study, through *in vitro* experiments and computational modelling, we show that I_{leak} affects iPSC-CM AP morphology, even above the R_{seal} values usually deemed acceptable in the literature. We show that R_{seal} cannot be easily compensated because it cannot be accurately measured during an experiment. Additionally, we posit that the background sodium current (I_{bNa}) in iPSC-CM models may be overestimated and mimic the effects of leak on AP morphology. Ultimately, we argue that leak current should be considered when interpreting, analysing, and fitting iPSC-CM AP data.

2 Methods

2.1 Modelling I_{leak}

We added a leak equation to the Kernik[13] and Paci[14] iPSC-CM and ToR-ORd[21] adult cardiomyocyte models. Knowing that leak acts as a depolarising current in iPSC-CM studies, and lacking information about specific charge carriers, we modelled I_{leak} as having a reversal potential of zero:[22,23]

$$I_{leak} = \frac{1}{R_{seal}} V = g_{seal} V,$$

where R_{seal} is the seal resistance and V denotes the membrane potential. The inverse of R_{seal} is the conductance, g_{seal}. Note that more complicated equations for leak current (non-linear, and/or with a non-zero reversal potential) may be required in experiments where CaF_2 seal enhancer is used.[24]

The effect of I_{leak} on the evolution of V was modelled as:

$$\frac{dV}{dt} = -\frac{1}{C_m}(I_{ion} + I_{leak}),$$

where I_{ion} represents the sum of transmembrane currents and C_m is the membrane capacitance. C_m was set to 50 pF (the experimental average from the cells used in the present study) for the Kernik and Paci simulations, and for ToR-ORd a value of 50 or 153 pF (the ToR-ORd baseline capacitance) was used unless specified otherwise.

2.2 Electrophysiological setup and data analysis

Perforated patch-clamp experiments were conducted following a previously described protocol (see Supplementary Methods for more details).[25]

After contact was made with a cell and a seal of >300 MΩ was formed, the perforating agent slowly decreased the access resistance to the cell (usually 10–15 minutes). This low R_{seal}

acceptance criterion was selected because we wanted to explore seal-leak effects above and below 1 GΩ. A series resistance (R_s) of 9–50 MΩ was maintained for all experiments. In this study, we used all cells from Clark et al.[25] with membrane resistance (R_m) and R_s measurements acquired before and after current clamp recordings and that did not produce spontaneous alternans (n=37 out of 40 cells). R_m, C_m, and R_s values were measured at 0 mV within one minute prior to the acquisition of current clamp data.

All AP features were calculated using a 10 s sample of current clamp data. The minimum potential (MP) was taken as the minimum voltage during this 10 s span. Maximum upstroke velocity (dV/dt_{max}), action potential duration at 90% repolarisation (APD_{90}), and cycle length (CL) were averaged over all APs in the 10 s sample.

2.3 R_{in} as an estimate of R_{seal}

We calculate R_{seal} using a small test pulse in voltage-clamp mode:[26]

$$R_{seal} = \frac{\Delta V_{cmd}}{\Delta I_{out}}.$$

Here, ΔV_{cmd} is the applied voltage step and ΔI_{out} is the difference in recorded current from before to during the step. Once access is gained to a cell it can be difficult to estimate R_{seal}, as the measured input resistance (R_{in}) depends on both R_m and R_{seal} (Equation 4, Figure 1). The effect of patch-clamp series resistance on R_{in} measures was excluded from Equation 4.

The smallest R_{seal} considered was 300 MΩ, while R_s values ranged from 9-50 MΩ. An increase of R_s from 9 to 50 MΩ (a worst-case scenario we never observed) for a cell with a 300 MΩ R_{seal} would change R_{in} by 13%. So, while R_s can change in these experiments, it is unlikely to affect R_{in} by more than a few percent, and R_{seal} is likely the predominant parameter affecting changes of R_{in}.

2.4 Additional methods

Additional methods can be found in the supplementary material.

3 Results

3.1 Leak affects iPSC-CM AP morphology even at seal resistances above 1GΩ

To investigate the effects of leak current on AP morphology, we simulated the addition of I_{leak} in the Kernik[13] and Paci[14] iPSC-CM models. Simulated AP recordings show that I_{leak} substantially alters AP morphology, even when $R_{seal} \geq 1GΩ$, a common threshold used in cardiac patch-clamp experiments.[20] For both models, decreases in R_{seal} depolarises the MP and causes a decrease in the dV/dt_{max}, likely due to an incomplete recovery of sodium channels at these depolarised MPs. Indeed, the Kernik model shows a transition to a small amplitude oscillation with very low upstroke velocity when $R_{seal}<3$ GΩ and then depolarised quiescence when $R_{seal}<2$ GΩ. I_{leak} effects on the APD_{90} differ for the two models — decreases to R_{seal} cause AP prolongation in the Paci model and AP shortening in the Kernik model. There are also differences in the effect of R_{seal} on CL: in the Kernik model, decreases in R_{seal} lead to a gradual decrease in CL, while in the Paci model decreasing R_{seal} initially has limited effect on CL, but then causes shortening as R_{seal} decreases below 5 GΩ.

3.2 Leak effects on adult cardiomyocyte APs are moderated by different current densities and increased ionic currents

The ToR-ORd adult cardiomyocyte model is also susceptible to I_{leak} effects, but the extent depends on cell capacitance (Figure 3). Simulations with C_m set to the average iPSC-CM capacitance (50 pF), result in substantial AP morphological changes when R_{seal} is between 1 and 2 GΩ. However, when C_m is set to a value in the range of adult human ventricular cardiomyocytes (153 pF) I_{leak} has little effect on AP morphology when R_{seal} is ≥1 GΩ (Figure 3B).

3.3 Rseal is not stable

Unlike voltage-clamp recordings, the effects of I_{leak} on AP morphology (measured in current clamp mode) cannot be corrected in post-processing. Current-clamp leak compensation is a potential solution to the issue,[22,23] but requires an accurate measure of R_{seal} throughout the experiment.

R_{seal} cannot be accurately determined after access is gained because measures are contaminated by R_m; such resistance measures are a composite of these two resistances that we nominally refer to as R_{in} (see Figure 1 and Methods). It is, therefore, tempting to measure the value before gaining access and assume it remains unchanged for the duration of an experiment. To investigate this, we considered *in vitro* R_{in} measures taken at two times during iPSC-CM experiments. R_{in} was measured with 5 mV steps from a holding potential of 0 mV (i.e., the leak reversal potential) before and after acquiring current clamp data. The data are skewed, with a mean of R_{in}=2.71 GΩ and median of R_{in}=0.82 GΩ.

The relative change in R_{in} from the first to the second time point was calculated and is plotted against the time elapsed between R_{in} measurements in Figure 4B. The median change of R_{in} is -15%. Because positive and negative changes cancel each other out in these statistics, we also inspected the absolute change, where we found a median of 20%. These data illustrate that R_{in} measurements often change over time. If we assume R_m is stable during experiments, this change in R_{in} should be attributed to R_{seal}, and suggests that the average cell's R_{seal} decreases (and therefore I_{leak} increases) over time.

3.4 R_{in} is not a good approximation of R_{seal} at any holding potential

A holding potential of −80 mV is a common choice for approximating R_{seal} with R_{in} measures. At this potential, sodium, calcium, and several potassium currents are expected to be largely inactive, but contributions from both I_{K1} and I_f must still be considered. Whilst I_{K1} is perhaps

close to its reversal potential (and therefore small), I_f is not and can play a large role at this voltage.

We recently showed that I_f is present in at least some of the iPSC-CMs used in this study.[25] I_f is also present in both the Kernik and Paci models, and we found the dynamics of the Kernik I_f model to be quite similar to the *in vitro* data in this study (Figure 5A-B). Figure 5A shows an example cell's response to an I_f-activating hyperpolarising step before and after treatment with quinine, at a concentration expected to lead to 32% I_f block (this data is taken from a section of a larger protocol — see Clark et al.[25] Figure 6A). A change in total current of nearly 2 A/F is observed after holding at −120 mV for 1 s (Figure 5A). In Clark et al.[25], nine cells were treated with quinine, and the average change during the I_f-activating segment was 1.34 A/F. We found that these nine cells could be sorted into three triplets based on the amount of quinine-induced I_{out} change during the I_f segment: no/little sensitivity (ΔI_{out} of 0-0.2 A/F), moderate sensitivity (ΔI_{out} of 0.7-1.2 A/F), and large sensitivity (ΔI_{out} of >1.9 A/F). Simulations using the Kernik model with 32% block of I_f show a change of 1 A/F (i.e., moderate change) in I_{out} (Figure 5B).

To illustrate the effect of I_f on leak calculations, we compared simulations from Kernik+leak models with R_{seal} = 1 GΩ and with g_f set to zero (i.e., not sensitive to quinine during hyperpolarizing step), the Kernik baseline value (g_f = 0.0435 nS/pF, i.e., moderate sensitivity), or twice its baseline value (g_f = 0.087 nS/pF, i.e., large sensitivity) (Figure 5C). We also reduced g_{K1} in these models to 10% of the baseline value to highlight the effects of I_f on R_{in} measures independent of I_{K1}. The calculated R_{in} values for these models at −80 mV are 2.03 GΩ for g_f=0 nS/pF (little change), 1.50 GΩ for g_f=0.0435 nS/pF (moderate change), and 1.16 GΩ for g_f=0.087 nS/pF (large change) (Figure 5C). These simulations show that, at −80 mV, I_f contributes to I_{out} and affects measures of I_{leak}.

Using these same models, we then calculated R_{in} values at multiple holding potentials between −90 and +30 mV to determine whether we could find a potential where R_{in} is close to R_{seal},

thereby minimizing the prediction error (Figure 5D). The model predicts that 20 mV (R_{in}=0.96 GΩ) minimises the error in our approximation of R_{seal}. This does not mean that R_{in} measurements at 20 mV will always produce the best estimate of R_{seal}. Instead, it indicates the size of I_{ion} does not change much when taking a 5 mV step from this potential. There is, however, a considerable amount of total current present, making this R_{seal} prediction sensitive to variations in the predominant ionic currents at this potential. Moreover, I_{leak} will be small and therefore more difficult to measure as 10 mV is close to the leak reversal potential (0 mV). It is also worth noting that the complex voltage- and time-dependent behaviour of transmembrane currents make R_{in} measures sensitive to both the duration and size of the voltage step (e.g., see supplement to Clerx et al.[27]). In summary, it is difficult to find a holding potential where R_{seal} can be measured without contamination from any transmembrane currents (i.e., where $I_{leak} = I_{out}$).

Taken together, these findings provide evidence to the claim that R_{seal} cannot be reliably measured in iPSC-CMs once access is gained.

Next, we compared the effect of I_f on R_m, and investigated the error in assuming $R_{seal} \approx R_{in}$, at both a 0 mV (i.e., I_{leak} reversal) and −80 mV holding potential. At 0 mV the Kernik+leak model is not sensitive to changes in g_f, as I_f is largely non-conductive (Figure 6A). However, due to an increased relative contribution of inward currents at 0 mV, the Kernik+leak model predicts a R_{in} with a large overestimation of R_{seal} (Figure 6B). This error increases as the true value of R_{seal} increases. Figure 6B also illustrates the sensitivity of the model to variations in g_f at −80 mV, with R_{seal} estimation errors decreasing as g_f increases; these errors also increase as R_{seal} increases. The improved prediction accuracy of the 0.087 nS/pF model at −80 mV is a coincidental side-effect of doubling g_f: with a different distribution of ion current densities or a larger baseline g_f value, the same doubling could just as easily worsen R_{seal} predictions. For example, the R_{in} of an iPSC-CM with a large I_{K1} current may slightly underestimate R_{seal} at −80

mV — doubling g_f in this case would result in a greater underestimation, increasing the error of the estimate.

3.5 C_m and R_{in}(0 mV) correlate with minimum potential

The iPSC-CMs used in this study displayed a heterogeneous phenotype (Figure 7), producing both spontaneously firing (n=25) and non-firing (n=12) current clamp recordings. Figure 7A shows three cells with very different baseline current-clamp recordings: non-firing and depolarised (grey), spontaneously firing with a short AP (black), and spontaneously firing with a long AP (blue). Non-firing cells (MP = −42 ± 8 mV) and cells with spontaneously-firing APs were depolarised (MP = −54 ± 7 mV) — the spontaneously-firing cells also had a shorter AP duration (APD_{90} = 128 ± 71 ms) (Figure 7B) relative to adult cardiomyocytes[28] and iPSC-CM models.[13,14]

We used linear regression analyses to determine if there is a correlation between g_{in}/C_m and AP biomarkers. Here, we use g_{in} (instead of R_{in}), as it reduces the spread of this variable and positively correlates with I_{leak} providing a more interpretable comparison with AP morphology. The values of each cell's g_{in} and C_m are shown in Figure 7C. I_{leak}'s effect on AP morphology is expected to scale directly with g_{in} and inversely with C_m. This is because g_{in}, even if a poor estimate, is expected to correlate with g_{seal} (Figure 6B)

A given g_{leak} will cause a smaller contribution in larger cells (i.e., cells with larger C_m), because the ionic currents are expected to scale with the size of the cell. For this reason, four AP biomarkers (MP, APD_{90}, CL, and dV/dt_{max}) were compared to g_{in}/C_m (Figure 8). The MPs of spontaneously firing ($R=0.44$, $p<.05$) and non-firing ($R=0.76$, $p<.05$) cells are positively correlated with g_{in}/C_m (Figure 8A). This finding is in agreement with our *in silico* studies showing that increasing g_{seal}, thereby increasing g_{in}, will depolarise the cell (Figure 2). The other three biomarkers failed at least one of the assumptions required when conducting a linear regression analysis (see Supplementary Methods). There are no obvious trends when comparing g_{in}/C_m to

CL or dV/dt_{max}. The APD_{90} plot, however, indicates there may be some AP shortening as g_{in}/C_m increases. Due to undersampling and a lack of linearity, we cannot make any claims of significance between these two measures. Leak simulations with the models, though correlated, did not predict a linear relationship between g_{seal} and these biomarkers (Figure 2C-D). However, the MP vs. g_{in}/C_m relationship passes all tests of linear regression assumptions and trends in the same direction as the Kernik and Paci simulations in Figure 2.

3.6 Fitting background currents in iPSC-CM models can absorb and imitate I_{leak}

We used optimization to study the potential of linear background currents (e.g., sodium and calcium) to imitate leak effects (see Supplementary Methods). We fit the baseline Kernik model to a Kernik+leak model with R_{seal} = 5 GΩ (Figure 9), allowing only the background sodium (g_{bNa}) and background calcium (g_{bCa}) conductances to vary. These currents were selected because they were incorporated into the Kernik model without independent iPSC-CM experimentation or validation. The best fit model had an increased g_{bNa} (×7.0), while g_{bCa} (×1.0) did not change much relative to the baseline model (Figure 9A). While not a perfect match, the best-fit trace reproduced qualitative features of the baseline+leak trace, showing a depolarised MP and a smaller amplitude (Figure 9B). This indicates that increased I_{bNa} can affect the AP in a fashion similar to I_{leak} such that mathematical iPSC-CM models may absorb I_{leak} effects by erroneously increasing background currents.

4 Discussion

Leak current is a common and unavoidable experimental artefact that affects patch-clamp recordings. In this study, using both model predictions and experimental data, we show that leak current: 1) affects iPSC-CM AP morphology; 2) can vary during experiments; 3) cannot be accurately estimated after access is gained to an iPSC-CM; and 4) may be absorbed by linear

equations for background currents when iPSC-CM models are fit to experimental AP data. During iPSC-CM current-clamp studies, leak consideration often starts with a pre-rupture seal measurement (with a 1 GΩ threshold) and is ignored if the seal appears to remain stable throughout the study. Here, we argue leak effects should be quantitatively scrutinised during the acquisition, analysis, and fitting of experimental data. Furthermore, we believe cell-to-cell variation in seal resistance contributes to observed iPSC-CM AP heterogeneity — often attributed nearly entirely to variations in ionic current densities.

4.1 Leak affects AP morphology

Simulations in chick embryonic cardiomyocytes, which are smaller than adult human cells (with model C_m = 25.5 pF), have previously shown that leak current substantially depolarises the MP and shortens the CL, even with R_{seal} values of 5 GΩ.[29] More recently, it was shown that *in vitro* iPSC-CMs were significantly depolarised during single-cell experiments, but not when cells were clustered.[11,12] These results indicate that isolated iPSC-CMs are likely affected by leak current. Our *in vitro* and *in silico* findings support this conclusion and strengthen the argument that iPSC-CM AP morphology is strongly affected by leak current.

Our *in silico* work indicates that I_{leak} has a smaller effect on recordings of adult cardiomyocyte AP morphology when compared to iPSC-CMs (Figure 3B). This effect is strongly modulated by C_m, indicating the larger size of adult cardiomyocytes has a moderating effect on I_{leak}-induced AP changes. When the I_{leak} artefact in this adult model is normalised by the average iPSC-CM capacitance (50 pF, Figure 3A), I_{leak} substantially alters the AP shape at R_{seal} values above 1GΩ. But the effects are much less than in the iPSC-CM model (Figure 2) — this indicates the ionic current expression profile of adult cardiomyocytes (e.g., greater I_{K1} and lower I_f density), in addition to cell size, moderates the effects of I_{leak} on adult AP recordings. Thus, differentiation strategies that aim to mature the iPSC-CM phenotype (both in size and ionic current expression) will likely produce cells that are affected less by I_{leak} artefact.

iPSC-CMs have long been defined by their immature and heterogeneous electrophysiological phenotype.[10,30] Such features are due, at least in part, to the types of ion channels expressed and cell-to-cell variations in ionic current conductances.[10,30] In this study, differences in the I_f responses to nine quinine-treated cells are an example of how iPSC-CM ionic currents can vary from one cell to the next. Heterogeneity in AP morphology and ionic current expression is also seen in primary adult cardiomyocytes.[31–33]

In this study, we show that I_{leak} also contributes to this immature and heterogeneous AP phenotype during single-cell patch-clamp experiments. The relative importance of I_{leak}'s influence on AP shape varies among cells, and depends on several factors, including: R_{seal}, C_m, and the ionic current expression profile. Simulations indicate that the AP shape can be substantially altered (relative to non-patched cells), even when R_{seal} is equal to 10 GΩ, an unrealistically high acceptance criterion for iPSC-CM patch-clamp studies. These factors, along with the potential for R_{seal} to change during an experiment, can confound drug and genetic mutation studies. For example, the irregular and depolarised phenotype (caused at least in part by I_{leak}) of iPSC-CMs in our recent cardiotoxicity study[25] made it impossible to measure consistent cell-specific changes in spontaneous AP morphology from pre- to post-drug application.

The AP-altering effects of I_{leak} can be effectively eliminated by patching cells while in an engineered heart tissue or monolayer. The electrical coupling of cells in these conditions results in an enormous effective capacitance, rendering I_{leak} an infinitesimal contributor to total current. While this eliminates the I_{leak} artefact, it also comes at a cost — this approach does not allow for the direct measure of APs in individual cells, limiting the ability to study iPSC-CM heterogeneity. In addition, it is not possible to acquire voltage clamp data from cells in these conditions — as such, one could not acquire both AP and descriptive data about individual currents, as we recently have done in isolated cells.[25]

4.2 Predicting R_{seal} during experiments

R_{seal} can be well-approximated prior to gaining access to a cell, but after perforation (or rupture) the presence of membrane currents make it impossible to obtain an accurate measurement (Figure 5). Our *in silico* work shows that, even when currents such as I_f and I_{K1} are reduced to <10% of their baseline values, R_{in} (measured at -80 mV) is still a poor approximation of R_{seal} (Figure 6, solid black line).

To address these difficulties, we believe it may be feasible to use the pre-rupture R_{seal} and post-rupture R_{in} measures to calculate estimates of R_{seal} during an experiment. This approach would require an accurate measure of R_{in} just after access is gained. Using R_{seal} and the initial R_{in}, it is possible to calculate R_m (Figure 1). An estimate of R_{seal} could then be made at any time during the experiment, assuming the calculated R_m stays constant, by re-measuring R_{in} and using Equation 4. This approach relies on two major assumptions: 1) the perforation/rupture step does not affect the seal; and 2) a protocol or procedure exists that can be used prior to each measurement of R_{in} to ensure that the contribution of R_m is consistent. We cannot say for certain that these assumptions will always be valid. However, we believe that recording frequent R_{in} measurements, estimating R_{seal}, and scrutinising changes are important steps for the correct interpretation of iPSC-CM current clamp data.

4.3 Correcting for R_{seal} during experiments

We believe these R_{seal} estimates should be used in a dynamic clamp leak compensation setup to address the limitations caused by a depolarised and variable MP. The approach works by injecting simulated currents into a cell in a real-time continuous loop during current clamp experiments.[34] I_{K1} dynamic clamp has been used on iPSC-CMs to attain quiescence at a MP below −70 mV so the cells can be paced at a desired frequency.[25,35–37] A dynamically clamped leak-compensation current has been implemented and used in manual patch-clamp studies with

neonatal mouse cardiomyocytes,[22] demonstrating the potential of using such an approach with small cardiomyocytes. The effects of leak and the ability of leak compensation to recover adult cardiomyocyte behaviour has also been demonstrated in an *in silico* study.[23] Together, these investigations demonstrate the potential of dynamic clamp as an experimental tool to simultaneously address shortcomings of the cells (i.e., I_{K1} density) and experimental setup (i.e., I_{leak}). This technique has the potential to improve the descriptive ability of iPSC-CMs when used in biophysical and drug investigations.

Inaccuracies in these estimates, however, will remain, resulting in the potential to under- or overcompensate. Overcompensation will hyperpolarise the MP and prolong phases 1 and 2 of the AP, so we believe undercompensation is preferable. We suggest injecting a fraction of the full compensatory current to mitigate the risk of underestimating R_{seal}. The Nanion Dynamite[8] sets the leak percent compensation to 70%, which seems reasonable.[38]

4.4 Models of background currents can incorporate leak artefacts

The Kernik and Paci iPSC-CM models took ion-specific background currents from the ten Tusscher et al.[39] model. These currents can trace their roots to the seminal work of Luo et al.[40], where they were included to help maintain physiologically realistic intracellular concentrations.

Direct measurements of I_{bCa} and I_{bNa} in iPSC-CMs have not been reported. The Kernik and Paci iPSC-CM models both adopted the ventricular[39] formulation for I_{bCa} and I_{bNa}, and then set the conductances of these currents by comparing model predictions of the AP with in vitro measurements in iPSC-CMs. We posit that I_{bNa} is overestimated and compensates for the explicit consideration of leak current artefacts, a source of discrepancy between these models and reality. We expect consideration of leak when constructing iPSC-CM models to reduce background sodium current and result in a more realistic model of intact iPSC-CMs.

4.5 Modelling experimental artefacts

While the effects of experimental artefacts in single-cell studies are well-established, consideration of them while building ion channel and action potential models has been limited.[41] *In silico* studies investigating series resistance effects on voltage clamp recordings have been done in fast-activating currents, such as I_{Na} and I_{to},[42,43] but to our knowledge artefact equations have not been included in the calibration process for widely-used models of these currents — although the I_{Na} model by Ebihara et al.[42] was incorporated directly into the widely copied I_{Na} model by Luo et al.[40]. Recently, Lei et al.[44] demonstrated that coupling experimental artefact equations with an I_{Kr} mechanistic model improved predictions. These studies show that including experimental artefact equations in model fitting can improve the descriptive ability of the resulting electrophysiological models. As such, we believe experimental artefacts should be explicitly considered at the modelling phase, and not ignored simply because a pre-determined minimum threshold is reached (e.g., 1 GΩ). Based on our findings, we believe cardiomyocyte models, and especially iPSC-CM models, should explicitly include leak currents when fitting to experimental current clamp data.

4.6 Recommendations

Our results provide important insights and recommendations for experimentalists and modellers alike:

1. *Experimental*: R_{seal} should be recorded before gaining access to a cell, and R_{in} measured frequently during an experiment. It is important to measure R_{in} from a voltage that provides a consistent measure of R_m, such that any changes in R_{in} can be attributed to changes in R_{seal}.
2. *Experimental*: Dynamic injection of a leak compensation current can help a cell recover its native AP, including the MP. Because R_{seal} is difficult to measure during experiments,

and to avoid overcompensation, we advise undercompensation (e.g., 70%). Additionally, R_{seal} and R_{in} measures should be reported.

3. *Modelling*: Explicit inclusion of I_{leak} will improve the descriptive ability of iPSC-CM models. While this may not always improve fits to AP data, it will take into account an important current affecting iPSC-CM recordings.

4.7 Limitations and future directions

This study has several limitations that should be considered during future investigations that may be affected by I_{leak}. First and foremost, when gathering these data for a previous study we did not follow our new recommendation of recording the exact value of R_{seal} before gaining access and then measuring R_{in} just after perforation. Going forward, we hope to use these two values to predict R_{seal} at multiple timepoints during an experiment, as outlined in Section 3.2. Second, we only conducted these experiments in one cell line. While our results appear similar to data from other labs,[11] it would be useful to conduct this study on multiple cell lines in the same lab. Third, we did not attempt dynamic injection of a leak compensation current — in future work we would like to investigate this as an approach to reducing cell-to-cell heterogeneity. Finally, the iPSC-CM models have innumerable differences from the cells used in this study, which is evident when comparing AP morpoholgies of *in vitro* cells (Figure 7A) to *in silico* models (Figure 2). However, agreement that we did see between simulations and our *in vitro* data demonstrate the potential of improving the descriptive ability of iPSC-CM models by including a leak current.

4.8 Conclusion

In this study, we demonstrate that leak current affects iPSC-CM AP morphology, even at seal resistances above 1 GΩ, and contributes to the heterogeneity that characterises these cells. Using both *in vitro* and *in silico* data, we showed the challenges of estimating R_{seal} after gaining

access to a cell and that R_{seal} is subject to change during the course of an experiment. We also posit that background sodium current in iPSC-CM models may be responsible for masking leak effects in *in vitro* data. Based on these results, we make recommendations that should be considered by anyone who collects, analyses, or fits iPSC-CM AP data.

5 Funding

This work was supported by: the National Institutes of Health (NIH) National Heart, Lung, and Blood Institute (NHLBI) grants U01HL136297 to D.J.C. and F31HL154655 to A.P.C.; the Wellcome Trust via a Senior Research Fellowship to G.R.M. (grant number 212203/Z/18/Z); the University of Macau via a UM Macao Fellowship and support from FDCT Macao (Science and Technology Development Fund, Macao S.A.R. (FDCT) reference number 0048/2022/A) to C.L.L.; the MKMD programme of the Netherlands Organization for Health Research and Development (grant number 114022502) to T.P.B.

6 Acknowledgements

We thank the members of our labs for their support and feedback at every step of the way.

7 Disclosures

T.P.B. is an Editorial Consultant of EP Europace and was not involved in the peer review process or publication decision. All remaining authors have declared no conflicts of interest.

8 Data Availability Statement

All data, code and models can be accessed from GitHub (https://github.com/Christini-Lab/iPSC-leak-artifact).

9 Translational Perspective

Human iPSC-CMs have emerged as a promising translational tool to study human cardiac physiology outside of the clinic. They have been particularly useful to investigate cell-level proarrhythmic substrates, including genetic mutations and ion channel-blocking drugs, and play a critical role as a model for validating drug effects on human whole-cell electrophysiology in the Comprehensive *in vitro* Proarrhythmia Assay (CiPA) initiative. However, the depth of insights from iPSC-CM data is often limited by inter- and intralab heterogeneity caused, at least in part, by patch-clamp experimental artefact. In this manuscript, we show how the seal-leak current is an often-overlooked artefact that confounds studies with iPSC-CMs. Ultimately, the findings and recommendations within this manuscript will improve the use of iPSC-CMs as an *in vitro* model to study cardiac electrophysiological diseases and patient-specific treatment strategies.

References

1. Terrenoire C, Wang K, Chan Tung KW, Chung WK, Pass RH, Lu JT, *et al.* Induced pluripotent stem cells used to reveal drug actions in a long QT syndrome family with complex genetics. *J Gen Physiol* 2013;**141**:61–72.

2. Han L, Li Y, Tchao J, Kaplan AD, Lin B, Li Y, *et al.* Study familial hypertrophic cardiomyopathy using patient-specific induced pluripotent stem cells. *Cardiovasc Res* 2014;**104**:258–69.

3. Mathur A, Loskill P, Shao K, Huebsch N, Hong SG, Marcus SG, *et al.* Human iPSC-based cardiac microphysiological system for drug screening applications. *Sci Rep* 2015;**5**:1–7.

4. Blinova K, Schocken D, Patel D, Daluwatte C, Vicente J, Wu JC, *et al.* Clinical Trial in a Dish: Personalized Stem Cell–Derived Cardiomyocyte Assay Compared With Clinical Trial Results for Two QT-Prolonging Drugs. *Clin Transl Sci* 2019;**12**:687–97.

5. Jæger KH, Wall S, Tveito A. Computational prediction of drug response in short QT syndrome type 1 based on measurements of compound effect in stem cell-derived cardiomyocytes. *PLoS Comput Biol* 2021;**17**:e1008089.

6. Jonsson MKB, Vos MA, Mirams GR, Duker G, Sartipy P, Boer TP de, *et al.* Application of human stem cell-derived cardiomyocytes in safety pharmacology requires caution beyond hERG. *J Mol Cell Cardiol* 2012;**52**:998–1008.

7. Goversen B, Heyden MAG van der, Veen TAB van, Boer TP de. The immature electrophysiological phenotype of iPSC-CMs still hampers in vitro drug screening: Special focus on I_{K1}. *Pharmacol Ther* Elsevier; 2018;**183**:127–36.

8. Mirams GR, Pathmanathan P, Gray RA, Challenor P, Clayton RH. Uncertainty and variability in computational and mathematical models of cardiac physiology. *J Physiol* 2016;**594**:6833–47.

9. Odening KE, Gomez AM, Dobrev D, Fabritz L, Heinzel FR, Mangoni ME, *et al.* ESC working group on cardiac cellular electrophysiology position paper: Relevance, opportunities, and limitations of experimental models for cardiac electrophysiology research. *Europace* 2021;**23**:1795–814.

10. Ma J, Guo L, Fiene SJ, Anson BD, Thomson JA, Kamp TJ, *et al.* High purity human-

induced pluripotent stem cell-derived cardiomyocytes : electrophysiological properties of action potentials and ionic currents. *Am J Physiol Hear Circ Physiol* 2011;**301**:2006–17.

11. Horváth A, Lemoine MD, Löser A, Mannhardt I, Flenner F, Uzun AU, *et al.* Low Resting Membrane Potential and Low Inward Rectifier Potassium Currents Are Not Inherent Features of hiPSC-Derived Cardiomyocytes. *Stem Cell Reports* 2018;**10**:822–33.

12. Van de Sande DV, Kopljar I, Maaike A, Teisman A, Gallacher DJ, Bart L, *et al.* The resting membrane potential of hSC-CM in a syncytium is more hyperpolarised than that of isolated cells. *Channels* Taylor & Francis; 2021;**15**:239–52.

13. Kernik DC, Morotti S, Wu H Di, Garg P, Duff HJ, Kurokawa J, *et al.* A computational model of induced pluripotent stem-cell derived cardiomyocytes incorporating experimental variability from multiple data sources. *J Physiol* 2019;**597**:4533–64.

14. Paci M, Hyttinen J, Aalto-Setälä K, Severi S. Computational Models of Ventricular- and Atrial-Like Human Induced Pluripotent Stem Cell Derived Cardiomyocytes. *Ann Biomed Eng* 2013;**41**:2334–48.

15. Koivumäki JT, Naumenko N, Tuomainen T, Takalo J, Oksanen M, Puttonen KA, *et al.* Structural Immaturity of Human iPSC-Derived Cardiomyocytes: In Silico Investigation of Effects on Function and Disease Modeling. *Front Physiol* 2018;**9**:80.

16. Es-Salah-Lamoureux Z, Jouni M, Malak OA, Belbachir N, Sayed ZR Al, Gandon-Renard M, *et al.* HIV-Tat induces a decrease in IKr and IKs via reduction in phosphatidylinositol-(4,5)-bisphosphate availability. *J Mol Cell Cardiol* Elsevier Ltd; 2016;**99**:1–13.

17. Garg P, Oikonomopoulos A, Chen H, Li Y, Lam CK, Sallam K, *et al.* Genome Editing and Induced Pluripotent Stem Cells in Cardiac Channelopathy. *J Am Coll Cardiol* 2019;**72**:62–75.

18. Ma D, Wei H, Lu J, Huang D, Liu Z, Loh LJ, *et al.* Characterization of a novel KCNQ1 mutation for type 1 long QT syndrome and assessment of the therapeutic potential of a novel I_{Ks} activator using patient-specific induced pluripotent stem cell-derived cardiomyocytes. *Stem Cell Res Ther* 2015;**6**:1–13.

19. Feyen DAM, McKeithan WL, Bruyneel AAN, Spiering S, Hörmann L, Ulmer B, *et al.* Metabolic Maturation Media Improve Physiological Function of Human iPSC-Derived Cardiomyocytes. *Cell Rep* 2020;**32**.

20. Herron TJ, Rocha AM Da, Campbell KF, Ponce-Balbuena D, Willis BC, Guerrero-Serna G, *et al.* Extracellular matrix-mediated maturation of human pluripotent stem cell-derived cardiac monolayer structure and electrophysiological function. *Circ Arrhythmia Electrophysiol* 2016;**9**:1–12.

21. Tomek J, Bueno-Orovio A, Passini E, Zhou X, Minchole A, Britton O, *et al.* Development, calibration, and validation of a novel human ventricular myocyte model in health, disease, and drug block. *Elife* 2019;**8**:1–48.

22. Ahrens-Nicklas RC, Christini DJ. Anthropomorphizing the mouse cardiac action potential via a novel dynamic clamp method. *Biophys J* Biophysical Society; 2009;**97**:2684–92.

23. Fabbri A, Prins A, Boer TP De. Assessment of the Effects of Online Linear Leak Current Compensation at Different Pacing Frequencies in a Dynamic Action Potential Clamp System. *Comput Cardiol (2010)* 2020;**2020**-**Septe**:1–4.

24. Lei CL, Fabbri A, Whittaker DG, Clerx M, Windley MJ, Hill AP, *et al.* A nonlinear and time-dependent leak current in the presence of calcium fluoride patch-clamp seal enhancer. *Wellcome Open Res* 2021;**5**.

25. Clark AP, Wei S, Kalola D, Krogh-Madsen T, Christini DJ. An in silico-in vitro pipeline for drug cardiotoxicity screening identifies ionic pro-arrhythmia mechanisms. *Br J Pharmacol* 2022;**179**:4829–43.

26. HEKA Elektronik GmbH. Patchmaster multi-channel data acquisition software reference manual. *Data Base* Holliston, MA,USA; 2016;**3304**:1–148.

27. Clerx M, Mirams GR, Rogers AJ, Narayan SM, Giles WR. Immediate and Delayed Response of Simulated Human Atrial Myocytes to Clinically-Relevant Hypokalemia. *Front Physiol* 2021;**12**:1–21.

28. O'Hara T, Virág L, Varró A, Rudy Y. Simulation of the undiseased human cardiac ventricular action potential: Model formulation and experimental validation. *PLoS Comput Biol* 2011;**7**.

29. Krogh-Madsen T, Schaffer P, Skriver AD, Taylor LK, Pelzmann B, Koidl B, *et al.* An ionic model for rhythmic activity in small clusters of embryonic chick ventricular cells. *Am J Physiol - Hear Circ Physiol* 2005;**289**:398–413.

30. Doss MX, Diego JM Di, Goodrow RJ, Wu Y, Cordeiro JM, Nesterenko V V., *et al.* Maximum diastolic potential of human induced pluripotent stem cell-derived cardiomyocytes depends critically on IKr. *PLoS One* 2012;**7**.

31. Ismaili D, Geelhoed B, Christ T. Ca2+ currents in cardiomyocytes: How to improve interpretation of patch clamp data? *Prog Biophys Mol Biol* Elsevier Ltd; 2020;**157**:33–9.

32. Lachaud Q, Aziz MHN, Burton FL, Macquaide N, Myles RC, Simitev RD, *et al.* Electrophysiological heterogeneity in large populations of rabbit ventricular cardiomyocytes. *Cardiovasc Res* 2022;3112–25.

33. Amos GJ, Wettwer E, Metzger F, Li Q, Himmel HM, Ravens U. Differences between outward currents of human atrial and subepicardial ventricular myocytes. *J Physiol* 1996;**491**:31–50.

34. Ortega FA, Grandi E, Krogh-Madsen T, Christini DJ. Applications of dynamic clamp to cardiac arrhythmia research: Role in drug target discovery and safety pharmacology testing. *Front Physiol* 2018;**8**:1–8.

35. Putten RMEM Van, Mengarelli I, Guan K, Zegers JG, Ginneken ACG Van, Verkerk AO, *et al.* Ion channelopathies in human induced pluripotent stem cell derived cardiomyocytes: A dynamic clamp study with virtual I_{K1}. *Front Physiol* 2015;**6**:1–16.

36. Goversen B, Becker N, Stoelzle-Feix S, Obergrussberger A, Vos MA, Veen TAB van, *et al.* A hybrid model for safety pharmacology on an automated patch clamp platform: Using dynamic clamp to join iPSC-derived cardiomyocytes and simulations of I_{K1} ion channels in real-time. *Front Physiol* 2018;**8**:1–10.

37. Li W, Luo X, Ulbricht Y, Guan K. Blebbistatin protects iPSC-CMs from hypercontraction and facilitates automated patch-clamp based electrophysiological study. *Stem Cell Res* Elsevier B.V.; 2021;**56**:102565.

38. Becker N, Horváth A, Boer T De, Fabbri A, Grad C, Fertig N, *et al.* Automated Dynamic Clamp for Simulation of I_{K1} in Human Induced Pluripotent Stem Cell–Derived Cardiomyocytes in Real Time Using Patchliner Dynamite8. *Curr Protoc Pharmacol* 2020;**88**:1–23.

39. ten Tusscher KHWJ, Noble D, Noble PJ, Panfilov A V. A model for human ventricular tissue. *Am J Physiol - Hear Circ Physiol* 2004;**286**:1573–89.

40. Luo CH, Rudy Y. A dynamic model of the cardiac ventricular action potential: I.

Simulations of ionic currents and concentration changes. *Circ Res* 1994;**74**:1071–96.

41. Whittaker DG, Clerx M, Lei CL, Christini DJ, Mirams GR. Calibration of ionic and cellular cardiac electrophysiology models. *Wiley Interdiscip Rev Syst Biol Med* 2020;**12**:e1482.

42. Ebihara L, Johnson EA. Fast sodium current in cardiac muscle. A quantitative description. *Biophys J* Elsevier; 1980;**32**:779–90.

43. Montnach J, Lorenzini M, Lesage A, Simon I, Nicolas S, Moreau E, *et al.* Computer modeling of whole-cell voltage-clamp analyses to delineate guidelines for good practice of manual and automated patch-clamp. *Sci Rep* Nature Publishing Group UK; 2021;**11**:1–16.

44. Lei CL, Clerx M, Whittaker DG, Gavaghan DJ, Boer TP de, Mirams GR. Accounting for variability in ion current recordings using a mathematical model of artefacts in voltage-clamp experiments. *Philos Trans A Math Phys Eng Sci* 2020;**378**:20190348.

Figure Legends

Figure 1: **R_{seal} cannot be measured directly once access is gained.** Once access is gained, we can only measure the combined resistance R_{in}, which is equal to the parallel resistances of R_{seal} and R_m (Equation 4). The presence of R_m introduces uncertainty when R_{in} is used to approximate R_{seal}, making it difficult to accurately correct for leak current effects. For simplicity, we have omitted other elements of this patch-clamp diagram (e.g., series resistance, capacitance, etc.).

Figure 2: **Effect of R_{seal} on Kernik and Paci APs.** Simulations from the Kernik+leak (**A**) and Paci+leak (**B**) models, each with capacitance set to 50 pF (the experimental average), and R_{seal} set to values from 1-10 GΩ. The dashed red trace shows a baseline (leak-free) simulation. Four

AP morphology metrics for the Kernik (**C**) and Paci (**D**) models are plotted against R_{seal} (displayed on log-scaled xaxis): minimum potential (MP), maximum upstroke velocity (dV/dt_{max}), action potential duration at 90% repolarisation (APD_{90}), and cycle length (CL). Grey boxes denote the R_{seal} values where the Kernik model is non-spontaneous.

Figure 3: **Effect of R_{seal} on ToR-ORd adult cardiomyocyte APs at 50 and 153 pF.** Simulations from the ToR-ORd+leak model paced at 1 Hz with Cm set to 50 pF (**A**) and 153 pF (**B**), and R_{seal} set to values from 1 to 10 GΩ. The dashed red trace shows a baseline (leak-free) simulation. Three AP morphology metrics for the 50 and 153 pF models are plotted against R_{seal} (displayed on log-scaled x-axis): MP, dV/dt_{max}, and APD_{90}.

Figure 4: **R_{in} changes during iPSC-CM experiments. A,** Distribution of initial R_{in} measurements from iPSC-CMs acquired with a +5mV step from 0 mV. **B,** The percentage change in R_{in} plotted against the time elapsed between R_{in} measurements. The interval between measurements ranged from 1 to 10 minutes. Time was recorded to the nearest minute, leading to the appearance of banding in the ΔTime measure.

Figure 5: **Ignoring the presence of I_f makes it impossible to accurately measure R_{seal} after gaining access. A,** Voltage clamp data acquired from an iPSC-CM before and after treatment with quinine, which is expected to block 32% of I_f at the concentration used. **B**, Kernik model response at baseline and with 32% block of I_f. **C**, Kernik+leak voltage clamp simulations conducted with R_{seal}=1GΩ, g_{K1} reduced by 90%, and g_f set to 0 (solid line), 0.0435 (dotted line), or 0.087 nS/pF (dashed line). A voltage step from −80mV to −75mV was applied, as is commonly used to estimate R_{in}. This R_{in} value is sometimes used to approximate R_{seal} when the holding potential is near −80 mV. The amplifier-measured (I_{out}), total transmembrane (I_{ion}), and leak currents (I_{leak}) are displayed. The R_{in} values calculated based on ΔI_{out} are 2.03, 1.50, and 1.16 GΩ for the 0, 0.0435, and 0.087 nS/pF simulations, respectively. **D,** R_{in} values are plotted

against holding potential for Kernik+leak models with R_{seal} = 1 GΩ and g_f equal to 0, 0.0435, or 0.087 nS/pF. The red dotted line shows the true simulated R_{seal} value of 1GΩ.

Figure 6: **R_{in} predictions of R_{seal} are overestimated at the reversal potential for leak current. A,** The current response (I_{out}) for Kernik+leak models with a 1 GΩ seal and g_f of 0 (solid line), 0.0435 (dotted line), or 0.087 nS/pF (dashed line) to a 50 ms +5mV voltage clamp step from 0mV (top) or −80mV (bottom). **B**, Effect of R_{seal} on R_{in} measures for models with g_f set to 0 (solid), 0.0435 (dotted), or 0.087 nS/pF (dashed). R_{in} was calculated with Equation 3. The +5mV voltage steps were taken from either 0 or −80 mV. The R_{seal} = R_{in} line (red dotted) is provided as a reference for when R_{in} correctly predicts R_{seal}. The 0mV lines are overlapping, illustrating that R_{in} is not sensitive to g_f at this voltage. The g_f=0.0875 nS/pF model at -80mV provides the best estimate of R_{seal}.

Figure 7: **Cells appeared phenotypically heterogeneous, with uncorrelated variation in g_{in} and C_m. A**, Current clamp recordings from three cells show phenotypic heterogeneity: non spontaneous (grey), spontaneous AP with short APD (black), and spontaneous AP with long APD (blue). **B**, MP and APD_{90} for spontaneously beating cells (n=25). Note the broken x-axis which allows us to display an outlying data point. **C**, The relationship between C_m and g_{in} for all cells (n=37). Non-spontaneous cell data points are denoted with squares while spontaneous are circles.

Figure 8: **Relationship between g_{in}/C_m and AP biomarkers. A**, g_{in}/C_m plotted against MP. Spontaneously firing cells are denoted as black points and non-firing cells as yellow squares. Linear regression fits to data from spontaneous (black dashed, R = 0.47, $p < 0.05$) and non-firing (yellow dotted, R = 0.76, $p < 0.05$) cells are overlaid on the plot. No statistically significant relationship was found between g_{in}/C_m and APD_{90} (**B**), CL (**C**), or dV/dt_{max} (**D**).

Figure 9: **A simulated example of how leak can be absorbed into background currents: Kernik baseline model fit to Kernik+leak model.** The I_{bNa} and I_{bCa} conductances (g_{bNa}, g_{bCa}) of the baseline Kernik model were fit to a Kernik+leak model (i.e., original+leak) with R_{seal} set to 5 GΩ using a genetic algorithm. **A**, The conductances for all individuals (grey) and the best fit individual (red square) from the last generation. **B**, Traces from the original baseline Kernik+leak model with a 5 GΩ seal (black), the best fit model from the last generation (red dashed), and the original baseline Kernik model (grey dotted).

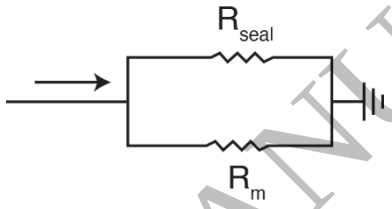

Figure 1
0x28 mm (x DPI)

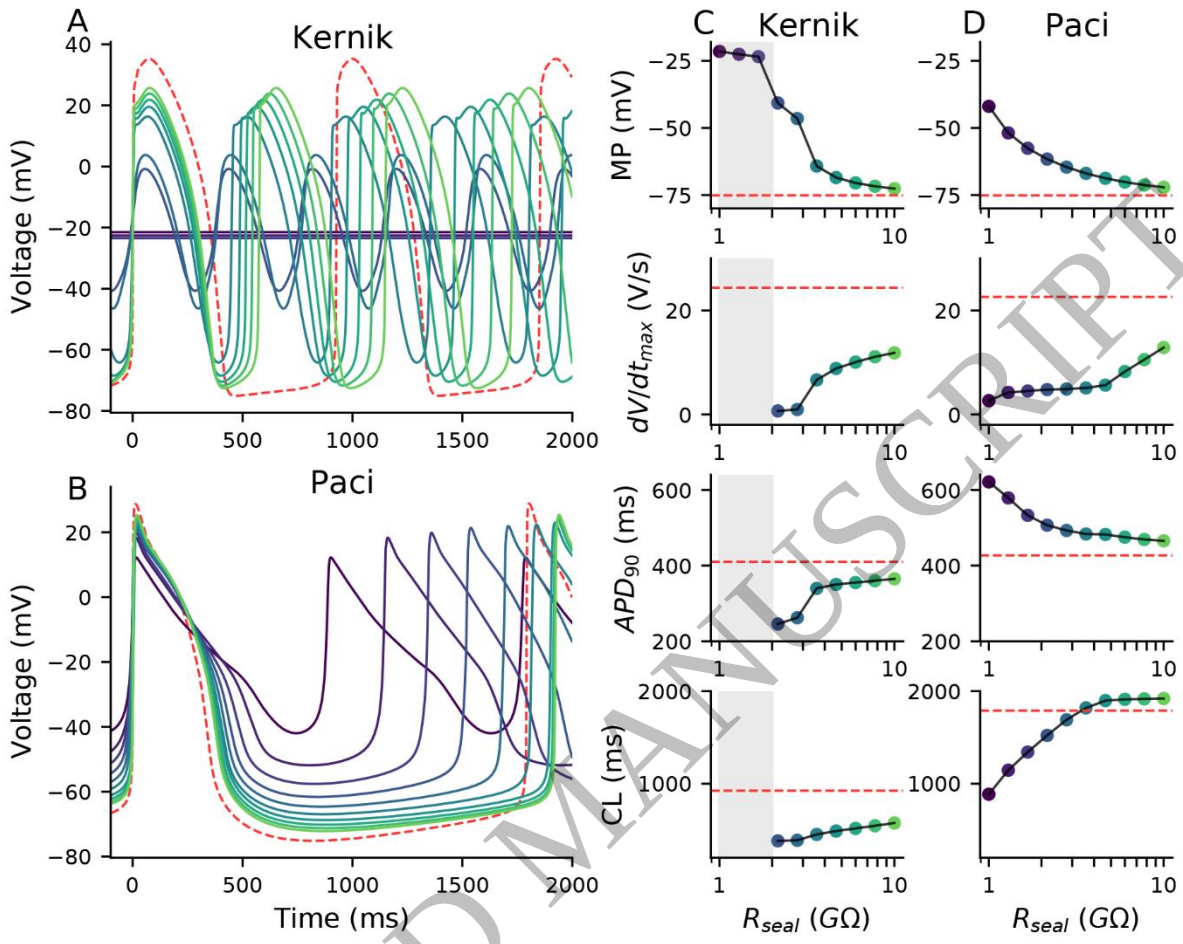

Figure 2
161x126 mm (x DPI)

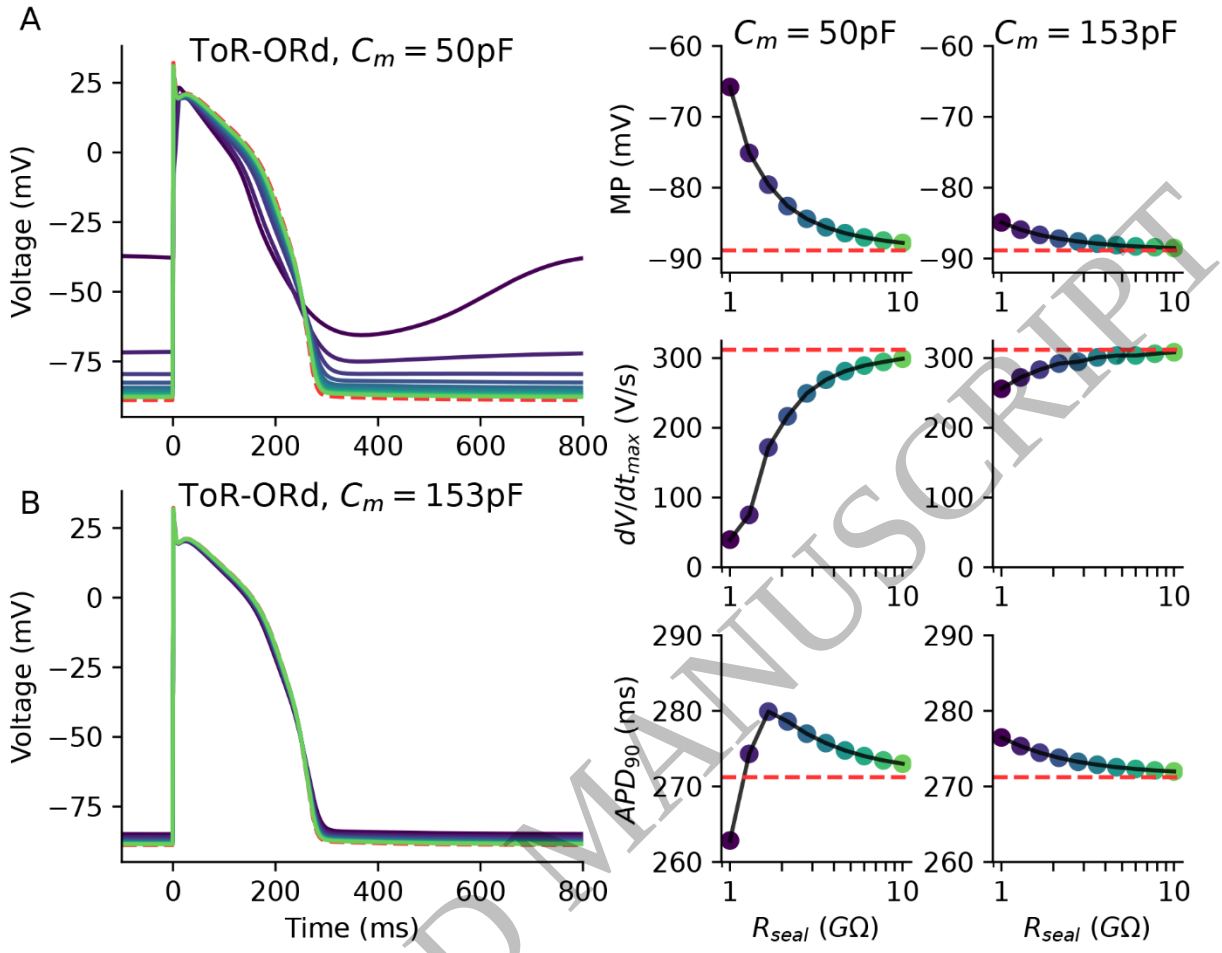

Figure 3
165x127 mm (x DPI)

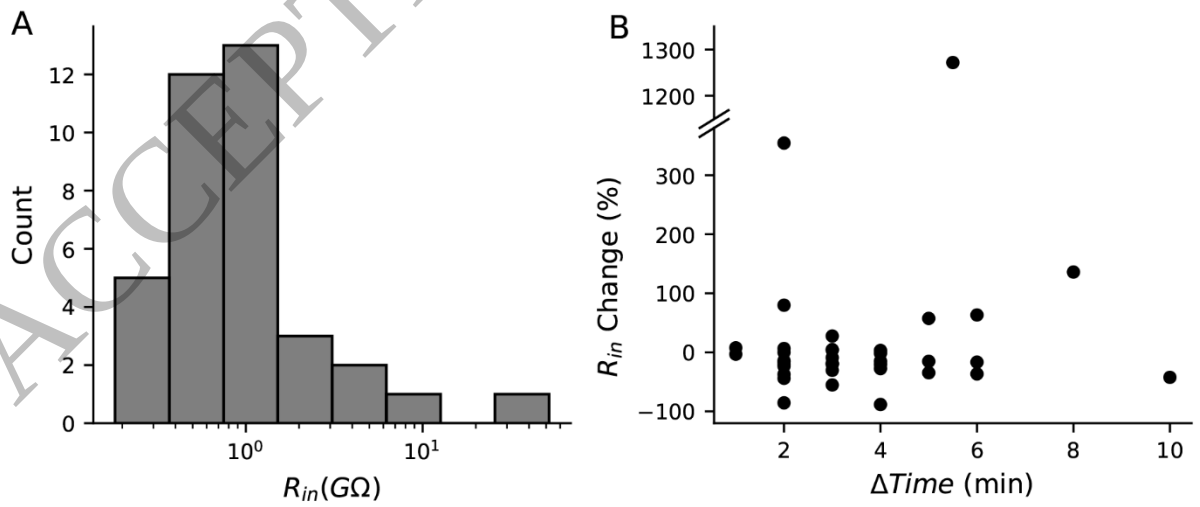

Figure 4
165x70 mm (x DPI)

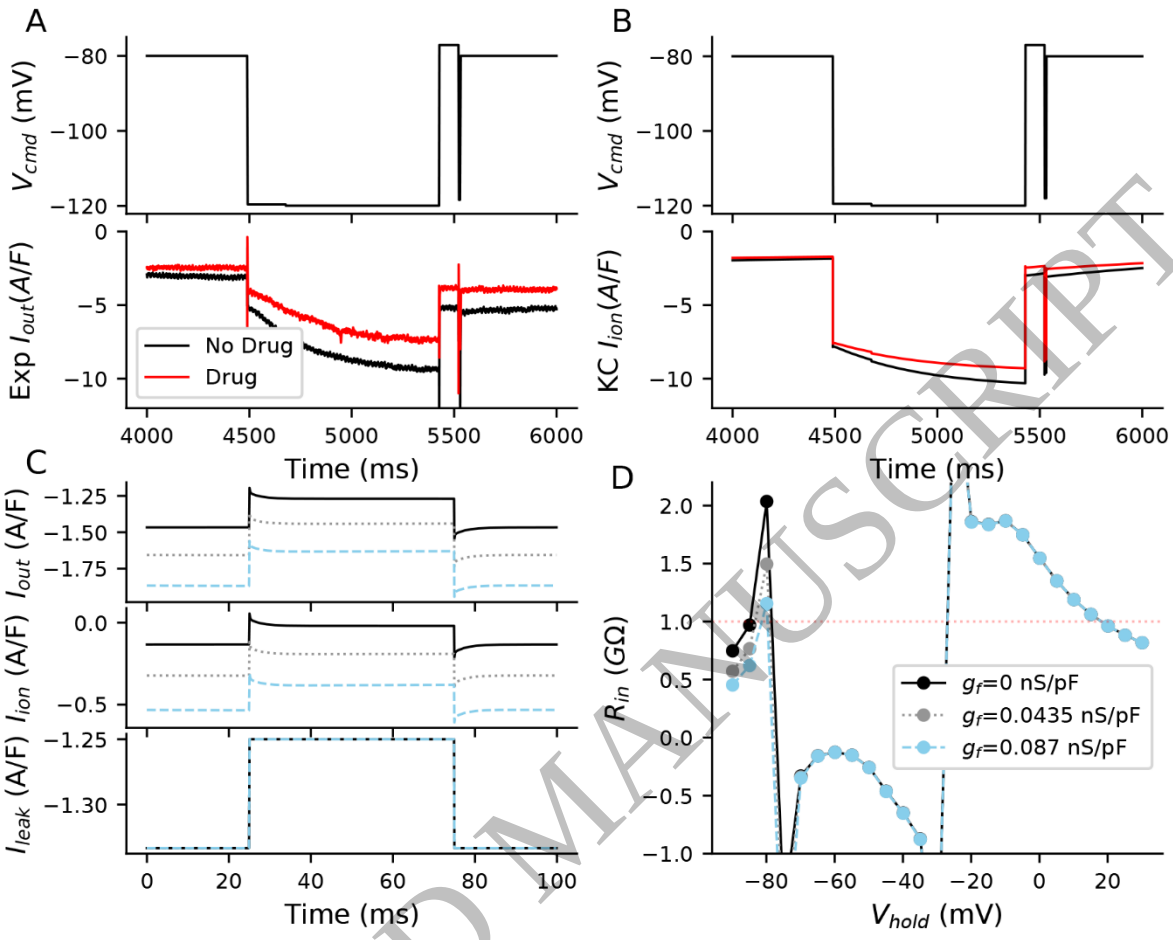

Figure 5
162x126 mm (x DPI)

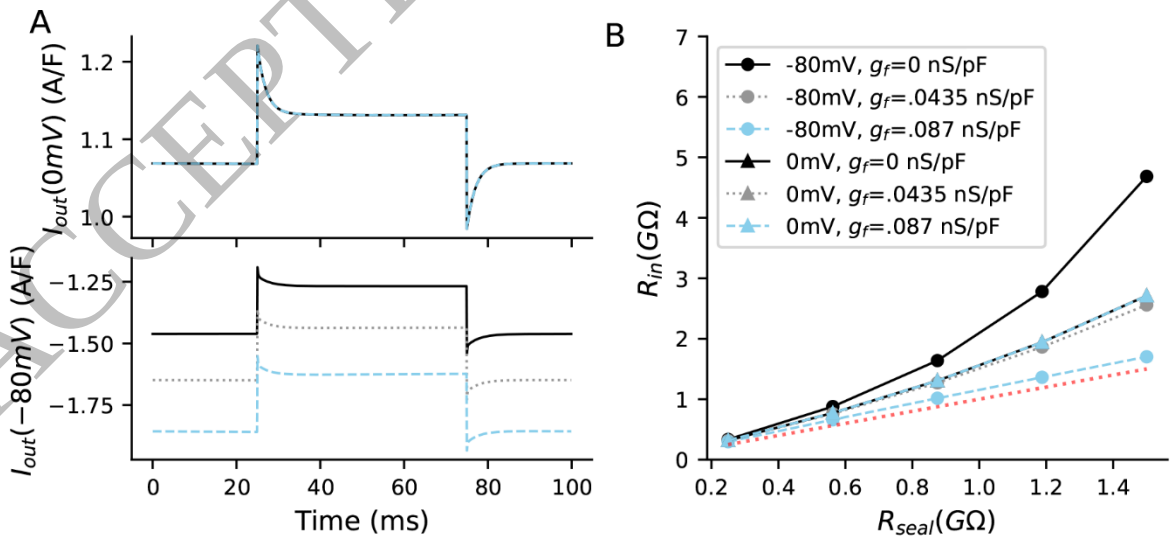

Figure 6
165x70 mm (x DPI)

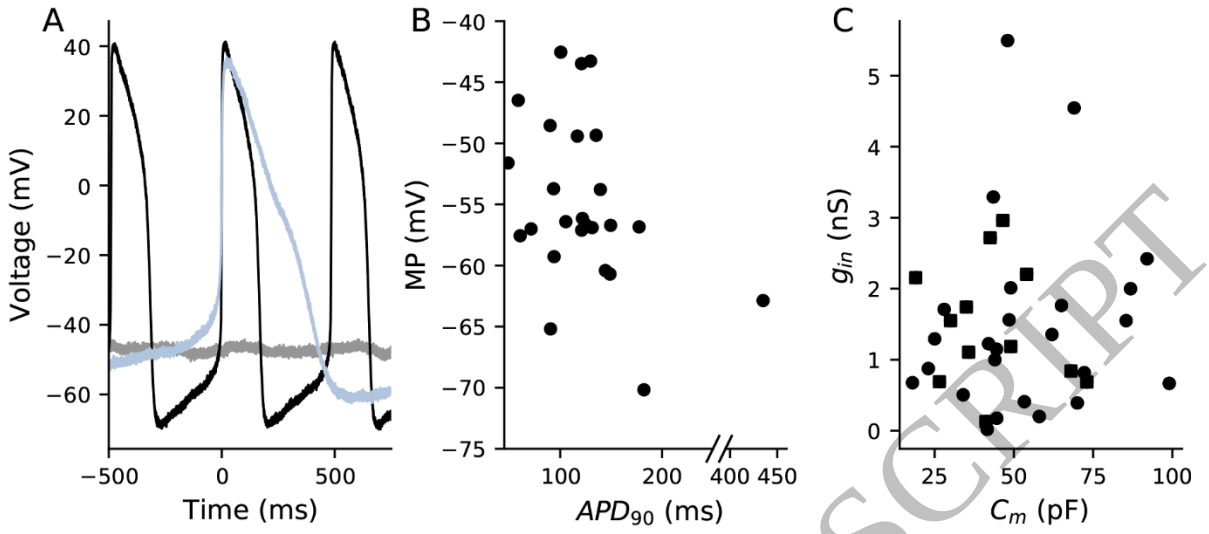

Figure 7
165x70 mm (x DPI)

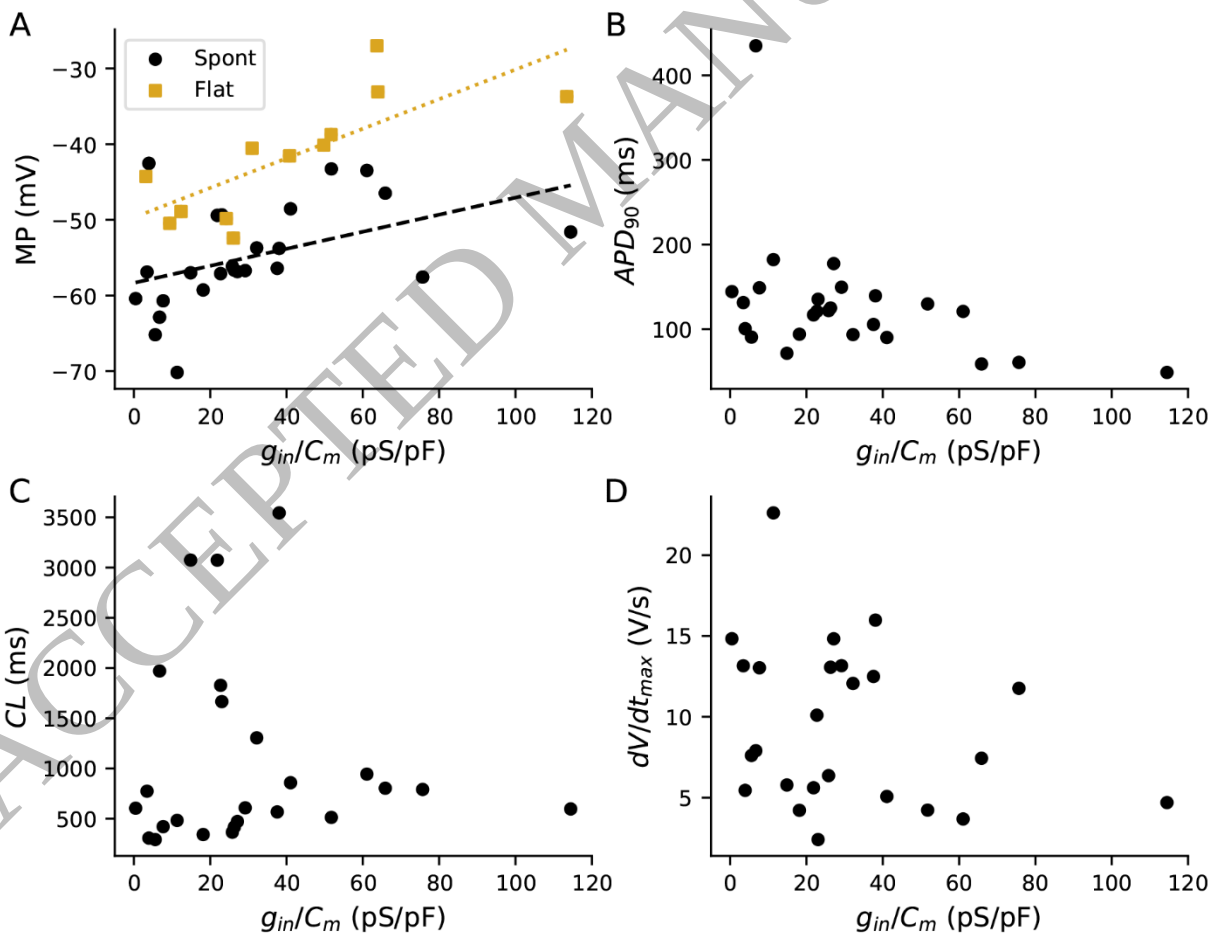

Figure 8
165x127 mm (x DPI)

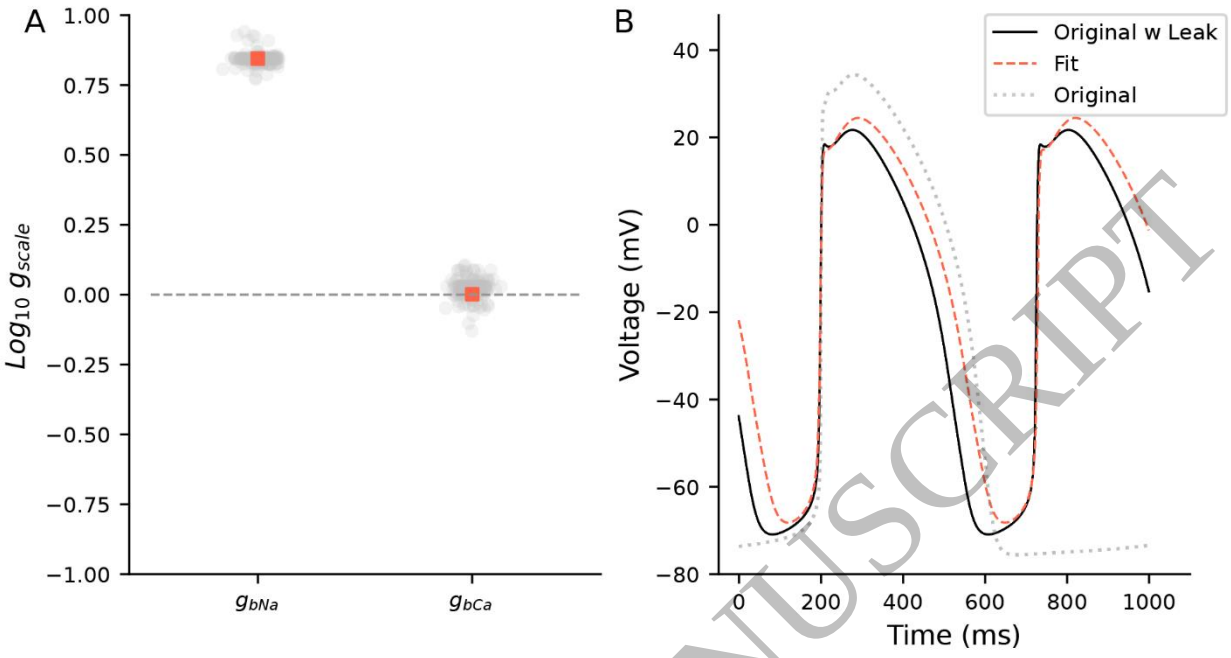

Figure 9
165x88 mm (x DPI)

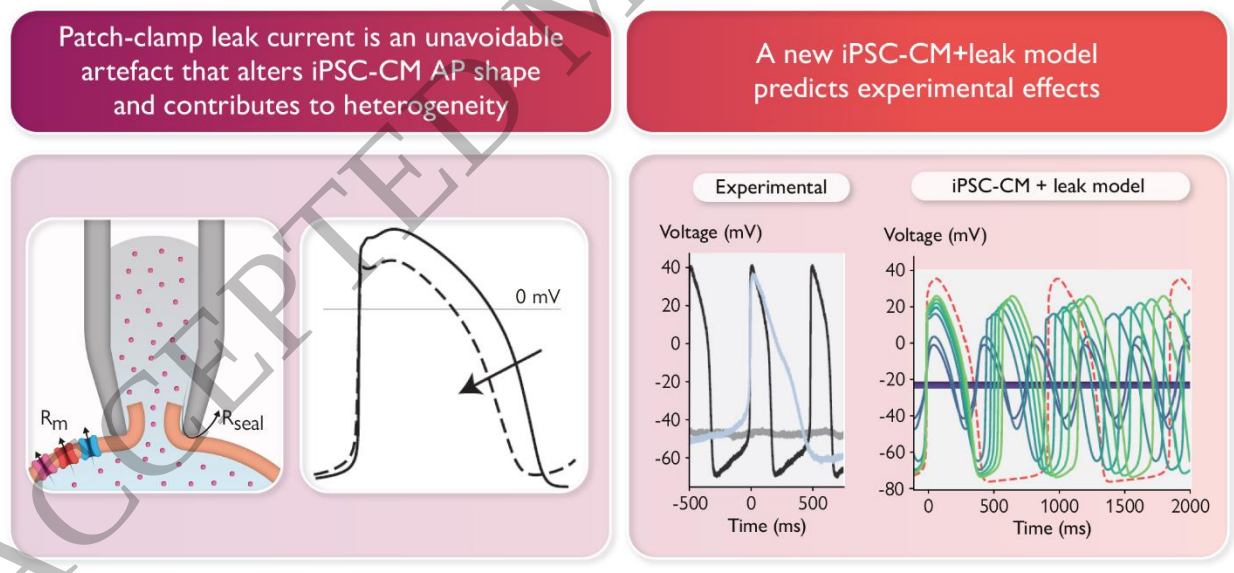

Graphical Abstract
165x76 mm (x DPI)